Correspondence and
requests for materials
should be addressed to
M.L. (marco.ligi@bo.
ismar.cnr.it)

# Post-Mesozoic Rapid Increase of Seawater Mg/Ca due to Enhanced Mantle-Seawater Interaction

Marco Ligi[1], Enrico Bonatti[1,2], Marco Cuffaro[3] & Daniele Brunelli[1,4]

[1]Istituto di Scienze Marine, CNR, Via Gobetti 101, 40129 Bologna, Italy, [2]Lamont Doherty Earth Observatory, Columbia University, Palisades, New York 10964, USA, [3]Istituto di Geologia Ambientale e Geoingegneria, CNR, c/o Dipartimento di Scienze della Terra, Sapienza Università di Roma, P.le A. Moro 5, I-00185 Rome, Italy, [4]Dipartimento di Scienze Chimiche e Geologiche, Università di Modena e Reggio Emilia, L.go S. Eufemia 19, 41100 Modena, Italy.

The seawater Mg/Ca ratio increased significantly from ~ 80 Ma to present, as suggested by studies of carbonate veins in oceanic basalts and of fluid inclusions in halite. We show here that reactions of mantle-derived peridotites with seawater along slow spreading mid-ocean ridges contributed to the post-Cretaceous Mg/Ca increase. These reactions can release to modern seawater up to 20% of the yearly Mg river input. However, no significant peridotite-seawater interaction and Mg-release to the ocean occur in fast spreading, East Pacific Rise-type ridges. The Mesozoic Pangean superocean implies a hot fast spreading ridge system. This prevented peridotite-seawater interaction and Mg release to the Mesozoic ocean, but favored hydrothermal Mg capture and Ca release by the basaltic crust, resulting in a low seawater Mg/Ca ratio. Continent dispersal and development of slow spreading ridges allowed Mg release to the ocean by peridotite-seawater reactions, contributing to the increase of the Mg/Ca ratio of post-Mesozoic seawater.

H as the composition of seawater changed through time? It appears that the Mg/Ca ratio of the Mesozoic ocean was 3 to 5 times lower than that of modern oceans[1-10] (Fig. 1a). Seawater Mg/Ca ratio is important as it affects the growth of calcitic versus aragonitic marine organisms, the deposition of inorganic carbonates (ooids, cements), as well as ocean-atmosphere $CO_2$ exchange, which influences climate.

A number of explanations have been suggested for the increase of the Mg/Ca ratio in post-Mesozoic seawater. One calls for a post-Mesozoic decrease of both the rate of Mg removal and of Ca release by the basaltic crust due to an alleged decrease in the rate of seafloor spreading and of hydrothermal circulation[11,12]. Another calls for enhanced deposition of dolomite that contributed to the late Mesozoic low seawater Mg/Ca ratio, followed by a decrease in dolomitization during the last ~ 100 Ma, due to lowering of sea level that restricted shallow seas where dolomitization is favored[1,6,7,9]. Post Mesozoic increased continental weathering has also been suggested[13], as it would increase the river input of Ca and Mg followed by preferential deposition of Ca as carbonates resulting in a Mg/Ca increase. These processes, although they can contribute to solve the problem, fail to explain satisfactorily the strong post-Mesozoic increase of seawater Mg/Ca[9,10]. We suggest here that seawater-mantle peridotite reactions in slow-spreading ridges may provide an important additional mechanism.

A number of processes affect the Ca and Mg content of the oceans. Present day average river input derived from continental weathering has been estimated at ~ $13.2 \cdot 10^{12}$ to ~ $15 \cdot 10^{12}$ mol/yr Ca and at ~ $5.2 \cdot 10^{12}$ to ~ $6.1 \cdot 10^{12}$ mol/yr Mg[1,6,14]. Before the discovery of subridge hydrothermal circulation no mechanism was known to get rid of Mg brought into the ocean by rivers[14]. During subridge high-T seawater circulation in the basaltic crust some Ca is extracted from basalt and added to seawater; in contrast, Mg is lost by seawater and incorporated into secondary minerals in the crust[15]. The quantity of seawater that goes through high-T hydrothermal circulation within the basaltic crust along today's mid-ocean ridges has been estimated at ~ $3–5 \cdot 10^{13}$ kg/yr (ref. 16). Geochemical (Li and Tl isotopes) and geophysical data[17,18] limit the high-T hydrothermal flux from the oceanic crust at ~ $1–3 \cdot 10^{13}$ kg/yr, in contrast with a flux of ~ $5–10 \cdot 10^{13}$ kg/yr necessary to balance the Mg oceanic budget[19]. Off-axis low-T alteration of the basaltic crust may affect significantly the budget of oceanic elements[20–22], including Mg, although Tl geochemistry[18] and estimates of off-axis basalt alteration[23] suggest little low-T basalt/ seawater chemical exchange at ridge flanks. Uncertainties in off-axis water fluxes[18,20] and variability in the chemistry of low-T off-axis hydrothermal fluids[21,22] make it difficult to estimate Mg fluxes at ridge flanks.
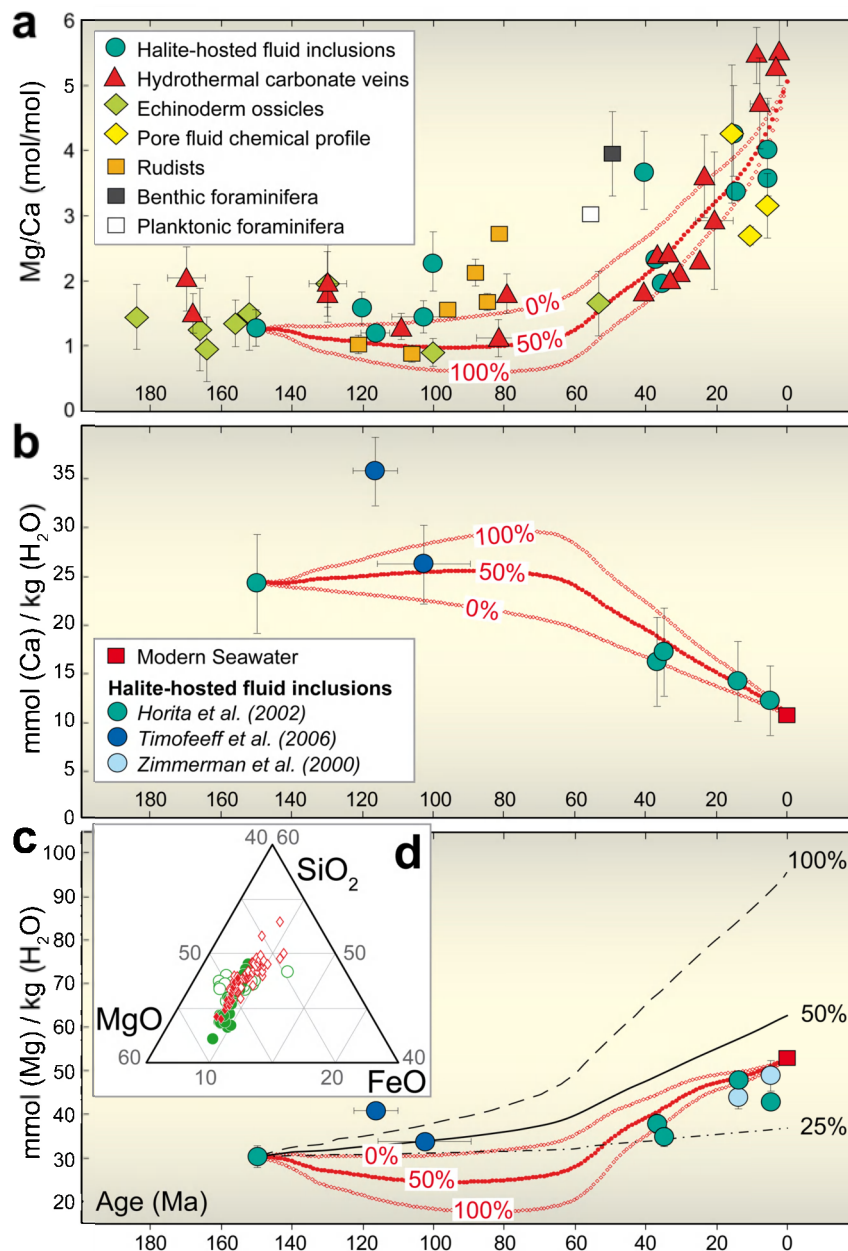
**Figure 1 | Seawater concentration of Mg and Ca.** (a), Estimates of Mg/Ca ratio of seawater since 180 Ma from ref. 10, including data from halite fluid inclusions (circles), ridge flank basalt carbonate veins[10,71] (triangles), echinoderm ossicles (green diamonds), pore-fluid chemical profile modelling (yellow diamonds), benthic and planktonic foraminifera (grey and white squares), and rudists[72] (yellow squares). The Mg/Ca temporal variations (red circles and diamonds) are obtained from models of secular variations of seawater concentration of Ca and Mg shown in (b) and (c), respectively. (b), Changes through time of seawater concentration of Ca versus variations in spreading rates and accretionary boundary geometry over the last 150 Ma, assuming an initial concentration of 24 mmol/kg (from brine inclusions in 150 Ma old evaporites[5]), and assuming constant river influx and residual outflow; variable Ca-release flux from hydrothermal circulation in basalt; and different degrees of Ca-removal variable-flux due to alteration of mantle rocks exposed at the seafloor (red filled circles and open diamonds). (c), Models of Cretaceous and Cenozoic changes in seawater concentration of Mg due to variations through time of oceanic crustal production and volume of mantle that can react at low-T with seawater (50%, red circles, 0% and 100% red diamonds), assuming constant river influx; variable Mg-release flux from low-T peridotite-seawater reactions; variable Mg-removal flux from high-T hydrothermal circulation in basalt; and a constant residual outflow, starting from an initial concentration of 30.5 mmol/kg at 150 Ma[5] and assuming a total seawater mass of $1.338 \cdot 10^{21}$ kg. Seawater Mg concentration due solely to Mg-release from MORP-seawater reactions for different volume fractions of peridotite interacting at low-T with seawater (25%, dashed-dotted line; 50%, solid line and 100% dashed line) is also shown. Red square is the modern seawater concentration. Blue and cyan circles are ancient seawater compositions calculated from measurement of fluid inclusions in marine evaporites[3,5,73]. (d), Triangular Mg-Si-Fe diagram showing the bulk composition of hydrated mantle-derived peridotites (open symbols) and reconstructed primary compositions of the same rocks (filled symbols). Diamonds refer to SWIR peridotites[34], circles to Vema Lithosperic Section peridotites[38,39]. Both populations show Mg-loss in serpentinites compared to unaltered primary peridotites.

Given a concentration of Mg in seawater of 0.053 mol/kg, and assuming high-T hydrothermal fluxes of ref. 16 extracting Mg totally from seawater, it follows that $\sim 1.6–2.7 \cdot 10^{12}$ mol/yr Mg are lost by seawater due to high-T hydrothermal flow. This Mg loss is a significant fraction of the yearly Mg river inflow into the oceans[20,24]. In addition, high-T hydrothermal reactions transfer $\sim 0.8–1.25 \cdot 10^{12}$ mol/yr Ca[6,15,20,24] from basalts to seawater.

Precipitation of carbonates from sea water is affected by temperature and seawater Mg/Ca ratio[2,7], with high Mg/Ca ratios favoring aragonite over calcite[31]. Deposition of dolomite extracts Mg from seawater at the rate of $1.7 \cdot 10^{12}$ mol/yr according to ref. 6.

## Results

Our suggestion that mantle peridotite-seawater relations have contributed to the post-Mesozoic increase of seawater Mg/Ca ratio is based on the following steps (see *Supplementary Information* for detailed explanations): (i) we modeled mantle dynamics beneath the global ridge system, showing that mid-ocean ridge peridotite (MORP) distribution depends on spreading rate. We assessed the volume of MORP that has the potential to react with seawater under conditions allowing Mg release; (ii) we demonstrated that MORP samples have lost Mg relative to their primary unaltered parent; (iii) we showed through global plate reconstructions how crustal production and average spreading rate have changed since the Cretaceous; (iv) we combined the results of (i), (ii) and (iii) to calculate the fluxes of Mg and Ca to the oceans as a result of mantle rock-seawater interactions, (v) we combined these results with estimates of the riverine and high-T hydrothermal Mg and Ca fluxes to model seawater Mg, Ca and Mg/Ca since 150 Ma (Fig. 1).

Significant stretches of today's slow-spreading ridges have mantle-derived peridotites emplaced either on, or at shallow levels below the sea floor, so that seawater can have access to the peridotites (Figs. 2 and 3). Peridotite-$H_2O$ reactions have been discussed in a large body of literature[25–29]. They can take place at temperatures up to $\sim 500°C$, with or without volume increase and elemental exchange[27], other than acquisition of $H_2O$ by the rock. Some reactions allow Mg to be released in solution[30]. In contrast to basalt-seawater hydrothermal reactions, when sea water reacts with peridotite Mg can be extracted from the rock, provided the temperature of the system is $< 150°C$ and water/rock (W/R) ratio is high[30–34].

Experiments[35] and numerical simulations[36] on olivine-$H_2O$ reactions show that Mg can be released in solution even at 300°C. Mg is also released by low-T dissolution of brucite, a phase likely to form during higher-T serpentinization, but hardly ever found in ocean floor serpentinites[25,30,34]. Low-T incongruent dissolution of olivine and enstatite may also release Mg[34,37].

### Modern MORP contribution to the ocean Mg and Ca budget.
In order to test if Mg is lost during reactions of seawater with MORP, we compared the chemical composition of primary unaltered MORP with that of hydrated MORP samples obtained at over 20 sites where mantle is exposed along the Vema Lithospheric Section in the central Atlantic[38,39]. They represent mantle residual after extraction of basaltic melt at a single segment of the Mid Atlantic Ridge (MAR) throughout 26 million years of crustal accretion. These rocks all contain $> 10\%$ $H_2O$. Their whole-rock primary major element content was calculated by combining their reconstructed primary modal composition with the chemical composition of the primary phases olivine, orthopyroxene, clinopyroxene and spinel (see *Supplementary Information*). We found that the altered peridotites, other than having gained $H_2O$ and lost some Si, have lost about 5–6% Mg relative to their unaltered parents (Fig. 1d). A similar loss of Mg due to reactions with seawater has been documented also in peridotites from the SW Indian Ridge (SWIR)[34] and from the Atlantis Massif (MAR at 30° N)[40]. A comprehensive major and trace element study of $\sim 130$ abyssal peridotite samples from Pacific and Indian ocean ridge–transform systems shows a mean $\sim 10\%$ wt% MgO loss relative to the MgO content of unserpentinized protoliths[41].

The extent to which ocean floor serpentinization implies volume increase is not settled yet. Textural analysis of thin sections of the
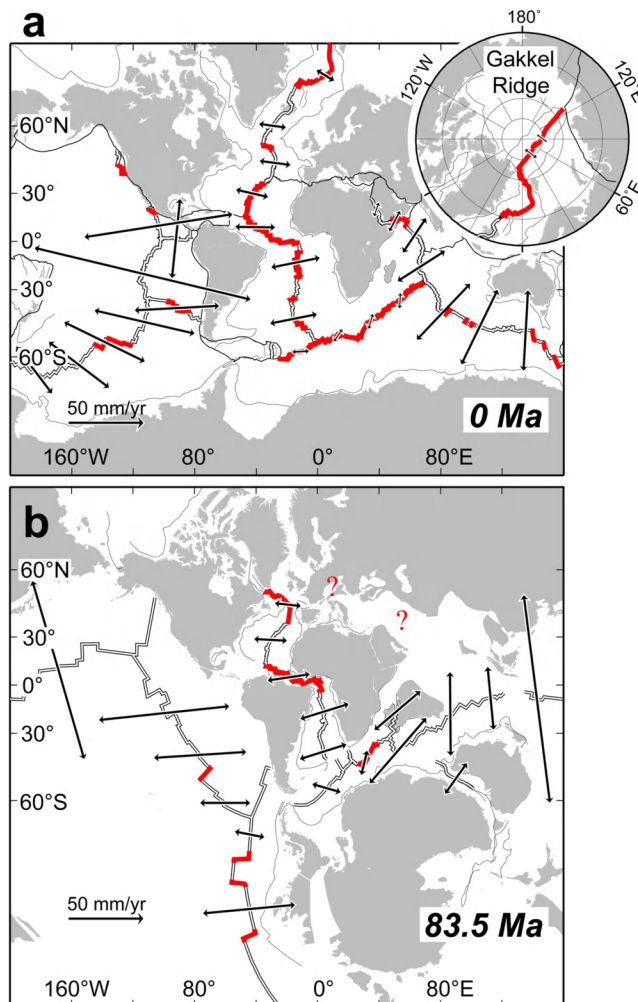


Figure 2 | Mantle seawater reactions at mid ocean ridges. (a), Present-day half spreading rates along mid ocean ridges, using relative plate kinematic models from ref. 45. Thick red solid lines indicate ridge segments, mostly with half spreading rate $< 10$ mm/yr, that can contribute to $<150°C$ MORP-seawater reactions and consequently to Mg release. The global ridge system was divided in 80 sectors each $2048 \times 1024$ km, partially overlapped to avoid edge effects. Assuming a plate spreading velocity for each sector by averaging spreading rates and directions, we calculated passive mantle flow, thermal structure and melt production beneath each ridge segment following methods of ref. 44. We calculated along-axis crustal thickness assuming pure-fractional melting and complete melt extraction. We neglected latent heat of fusion by melt freezing and hydrothermal cooling. The along-axis depth-distribution of the 150°C isotherm was obtained by averaging depths from 10 km-wide across-axis sections. The integral of differences between isotherm depth and crustal thickness (where they are positive) times the full spreading rate gives us an estimate for each ridge segment of the volume of mantle-derived MORP that can interact yearly with seawater at a temperature below 150°C. (b), Half spreading rates along mid-ocean ridges at 83.5 Ma, obtained using digital models for spreading velocities from refs. 47 and 48. Half spreading rate was generally faster than 15 mm/yr, implying little or no MORP-seawater reactions. Reconstructed positions of continents at 83.5 Ma (Santonian), relative to Africa assumed to be fixed, were obtained with the Gplates software (http://www.gplates.org).
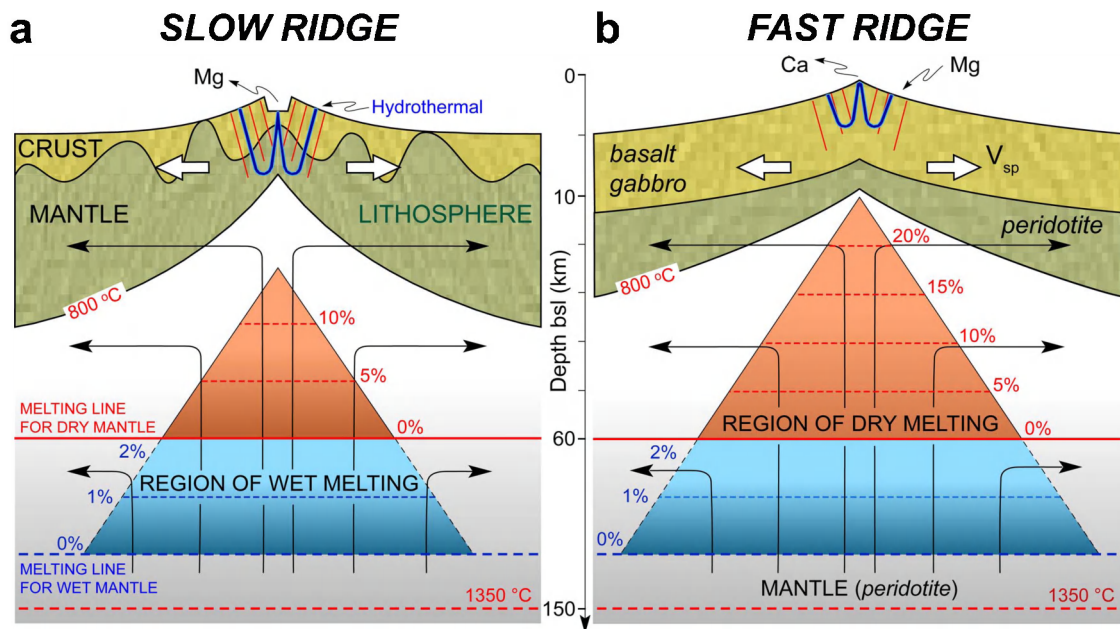
**Figure 3 | Effects of spreading rate on the possibility of MORP-seawater reactions during hydrothermal circulation at mid ocean ridges.** Assuming a constant mantle potential temperature of 1350°C at a depth of 150 km and plate thickening passive flow, the degree of melting of the upwelling mantle depends on whether plate separation is slow (a) or fast (b). We solved for the steady-state three-dimensional passive mantle flow via a Fourier pseudo-spectral technique[44]. The base of rigid plates, assumed to correspond to the depth of the 800°C isotherm, was obtained iteratively solving each time the mantle temperature field, starting from a constant-thickness plate-flow model. Streamlines show a schematic passive corner flow in the asthenosphere. The shaded triangles indicate the fraction of melt generated across axis, including the effect of water on peridotite solidus. Assuming a ~ 0.02 wt% $H_2O$ content in the upper mantle, the peridotite solidus is lowered causing partial melting in a subridge mantle region wider and deeper than if the mantle were dry. The faster the mantle rises, the shallower melting ends. As a result, more mantle melts, creating a thicker basaltic crust and shallow seawater penetration, with little chance for mantle ultramafics to interact with seawater and to release Mg to the ocean. Slow ridge MORP-seawater reactions may result in Mg release to the ocean.

Vema serpentinites suggest that volume increase during serpentinization was limited to <20%. Similar low volume increase was estimated for Atlantis Massif serpentinites[42], implying significant Mg loss[25,30]. Nevertheless, Mg-bearing fluids derived from low-T hydrothermal circulation in mantle peridotites have not been reported to date, consistent with bulk-rock Mg depletion being probably related to low-T "pervasive weathering" by seawater of a relatively thick ultramafic zone[34,41]. However, the issue of Mg-loss versus temperature during MORP-seawater reactions is constrained by the temperature below which the reacting fluid is undersaturated in Mg-rich minerals (i.e., < 150°C following ref. 34), independently of the process leading to Mg-depletion of MORPs (i.e., near constant-volume mantle hydration or pervasive "marine weathering").

We estimated next the potential for peridotite-seawater reactions in the modern versus Cretaceous-Cenozoic oceans (Fig. 2). Seawater-MORP reactions require: (a) thin (or absent) basaltic crust; (b) sub-seafloor seawater penetration (unless peridotites are exposed directly on the seafloor); (c) temperature below the 500°C isotherm (150°C to favor Mg release).

Basaltic crust thickness is related to subridge thermal structure and increases with spreading rate[43]. We calculated it (see *Supplementary Information*) following computational methods on plate-driven subridge mantle flow for a lithosphere that thickens with age[11] (Fig. 4). We considered the global mid-ocean ridge system using the current plate motion model of ref. 45. Half spreading rates, ranging from 3.9 mm/yr (i.e. Gakkel Ridge) to 75 mm/yr (i.e. East Pacific Rise), were used to calculate mantle flow velocity. Crustal thickness increases rapidly with half spreading rate from 0.5 to 8 km, whereas subridge seawater penetration, inferred from the depth of faults deduced from seismic hypocenters, decreases as spreading rate increases[46] (Figs 3 and 4). We applied similar procedures to reconstruct

paleo-oceans. Plate tectonic reconstructions, based on plate boundaries and finite Euler vectors from refs. 47 and 48, were calculated for several Chrons (see *Supplementary Information*) since the Late Oxfordian (154.3 Ma).

The subridge distribution of isotherms is related to mantle's potential temperature, spreading rate and vicinity to transform offsets. The 150°C subridge isotherm rises with spreading rate: it lies < 0.5 km deep below mid-segment points at fast ridges versus > 4 km at ultra-slow ridges. At ridge-transform intersections it deepens depending on the age contrast, i.e., offset length and slip rate. One example is in the equatorial MAR where a mantle thermal minimum, enhanced by a long transform "cold edge effect", determined nearly amagmatic accretion and an ultramafic seafloor along a ~ 40 km long ridge segment[49,50].

Exposure of MORP at the seafloor, with the possibility of peridotite/seawater reactions, is favored by vertical tectonics triggered by low-angle detachment faults and core complexes, common in slow-spreading ridges[40,51–53], as well as by transtension/transpression along transforms due to small changes in ridge/transform geometry[38,54]. These processes may affect significant portions of the MAR with peridotites making up as much as 75% of the deeper rocks exposed[52,53,55]. In addition, significant stretches of slow ridges (i.e., Gakkel Ridge, SWIR, MAR) expose ultramafics along axis, away from transforms and core complexes[48,49,56,57]. Overall, up to 20% of the seafloor at modern mid ocean ridges may be floored by peridotites.

These factors (Fig. 4) suggest that mantle-derived MORP can interact with seawater only at half spreading rates <12 mm/yr (other than close to long transform intersections), i.e., in stretches of the mid Atlantic, Indian, American-Antarctic and Gakkel Ridges, but not along the fast-spreading East Pacific Rise (Fig. 2a), except in a few peculiar tectonic settings, i.e., Hess Deep[58] and the Garret
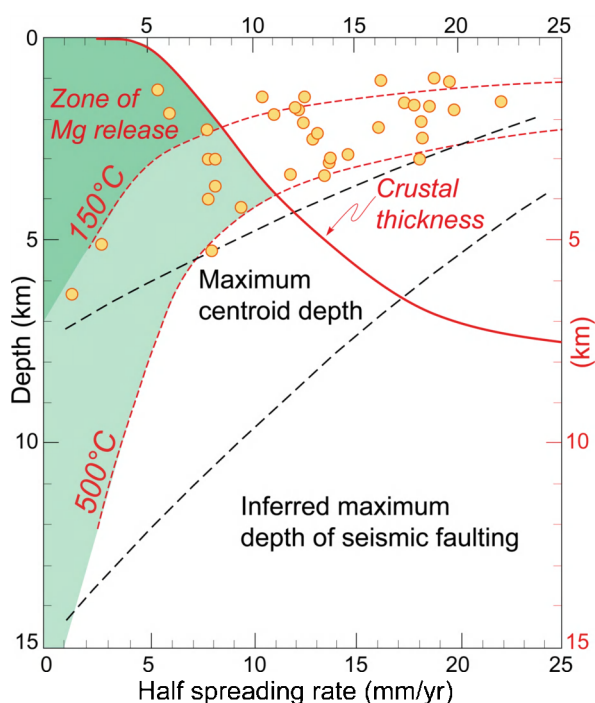
**Figure 4 | Zone below mid ocean ridges where mantle-seawater reactions are possible.** Basaltic crustal thickness increases with spreading rate, while depth of seawater penetration, inferred from earthquake hypocenters (yellow filled circles), decreases with spreading rate. The subridge zone with potential MORP-seawater reactions is indicated. Serpentinization, limited by the 500°C isotherm, is possible (other than close to long offset transforms) in ridges with half spreading rate < 12 mm/yr. MORP-seawater reactions at <150°C, where Mg-release is possible, are limited to ridges with half spreading rate < 8 mm/yr. Predicted crustal production and depth of the isotherms, obtained simulating two plates diverging along a mid ocean ridge, are indicated as red solid and dashed lines, respectively.

Transform[59]. Adding up the slow-ultraslow-spreading ridge stretches, we estimate that approximately $9.2 \cdot 10^{11}$ kg of mantle-derived MORP can interact yearly with seawater at T < 150°C and can potentially release Mg to the oceans. In places along slow mid ocean ridges, parts of layer 3 may be serpentinites instead of gabbros, both with a P-wave seismic velocity of ~ 6 km/s (*Supplementary Fig. S3*). Exposure of (sub-continental) mantle peridotites occurs also in magma-poor ocean-continent transition, as across the W-Iberian margin[60]. The zone of serpentinized peridotite along the W-Iberian margin is up to 6 km thick[60], suggesting important alteration and serpentinization at depth.

We estimated next the quantity of Mg contributed to the modern ocean by MORP-seawater reactions. If 100% of MORPs that can potentially react with seawater at < 150°C do actually react and lose at least 5% wt of MgO, seawater will gain $1.15 \cdot 10^{12}$ mol/yr Mg. This is ~ 20% of the yearly Mg river input. If only 10% react, seawater will gain $1.15 \cdot 10^{11}$ mol/yr Mg, i.e., ~ 2% of the river input. Mg release by MORP-seawater reactions requires high water/rock ratios. Assuming W/R ratios from 10 to 10,000, the fluxes of $H_2O$ required to mobilize $1.15 \cdot 10^{12}$ mol/yr Mg (100% of MORPs) range from ~ $10^{13}$ to $10^{16}$ kg/yr (i.e., close to or higher than the ridge high-T hydrothermal flux in basaltic crust). This is consistent with the total length of modern slow/ultraslow spreading ridges exceeding the length of fast spreading systems, and with larger volumes of rock being involved in low-T hydrothermal circulation.

Moreover, ridge stretches where MORPs prevail imply a decrease of the ridge length where hydrothermal seawater reacts with basalt, lowering both the quantity of Mg extracted from seawater, and of Ca

released to seawater (Fig. 1b and 1c). Although, low-T MORP-seawater reactions at ridge flanks may be significant sources of Mg, we did not consider them, as they are difficult to quantify. We also did not consider contributions from non-volcanic passive margins, and supra-subduction zones.

**Scarcity of peridotite-seawater reactions in the Mesozoic Mega-ocean.** Let us consider if and how the factors outlined above were different in the late Mesozoic, to see if they can explain the low Mg/Ca ratio of Mesozoic seawater. Continents assemble in a single supercontinent and then gradually disperse again in ~ 500 million years Wilson cycles. A single supercontinent (Pangea) dominated the scene in the early Mesozoic[61]. This implies a single super-ocean (Panthalassa), a sort of super-Pacific, but hardly any intercontinental, Atlantic/Indian/Arctic-type oceans.

The super-ocean was at first probably almost surrounded by subduction boundaries and must have involved a fast-spreading "hot" mid ocean ridge system, generating a > 5 km thick basaltic crust, shallow 150°C and 500°C isotherms and shallow hydrothermal penetration, with little or no chance for mantle ultramafics to interact with seawater and to release Mg to the ocean. On the contrary, the Mesozoic super-ridge was probably the locus of intense high temperature hydrothermal circulation within the thick basaltic crust, with Mg being drained from, and Ca contributed to, seawater. Tethys, the only significant Cretaceous intercontinental ocean, hosted ridges that mostly spread faster than 20 mm/yr[62], thus with no significant MORP-seawater reactions (Fig. 5).

Seawater Mg/Ca temporal variations are paralleled by changes of $\delta^{11}B$ (ref. 24). $^{10}B$ is extracted from seawater preferentially to $^{11}B$ during hydration of mantle peridotites[63]. Thus, a $^{11}B$ increase in post-Mesozoic seawater, in parallel with the increasing importance of peridotite-seawater reactions, is consistent with our model.

Mg isotopes may help in assessing the extent to which MORP-seawater reactions have contributed Mg to seawater. The $\delta^{26}Mg$ of river input is today ~ $-1.09‰$, different from that of seawater ($-0.82‰$)[64]. The $\delta^{26}Mg$ of oceanic basalt is $-0.36‰$; given that no isotopic fractionation occurs during partial melting[65], MORP should have a similar $\delta^{26}Mg$. Release of Mg from MORP to seawater, assuming no isotopic fractionation, should increase the $\delta^{26}Mg$ of seawater relative to that of rivers, i.e., the difference between seawater and river water would become larger. In contrast, basalt-seawater interaction should not alter significantly seawater $\delta^{26}Mg$, assuming that Mg is entirely trapped by basalt or no isotopic fractionation during Mg-removal by hydrothermal circulation. We predict that the $\delta^{26}Mg$ of Mesozoic seawater (little Mg input from MORP) was more negative than the $\delta^{26}Mg$ of modern ocean (significant input from MORP). However, dolomite deposition, given that dolomite $\delta^{26}Mg$ ($\sim -2‰$) is more negative than that of rivers[64], will also drive seawater $\delta^{26}Mg$ towards less negative values, just as MORP-derived Mg would. Calculations on MORP-driven versus dolomite-driven changes of seawater $\delta^{26}Mg$ suggest that modern ocean $\delta^{26}Mg$ is affected significantly by MORP-derived Mg (see *Supplementary Information*).

Weathering of continental rocks probably contributed a lower quantity of both Ca and Mg to the ocean during a "supercontinent" stage relative to a "dispersed continents" stage. A relatively low $^{87}Sr/^{86}Sr$ ratio of Jurassic carbonates[66] supports this statement. However, a lower river input of Ca and Mg does not imply a different Mg/Ca ratio, given that the overall composition of the "dispersed continents" should not be very different from that of the "supercontinent".

**Mg/Ca in post Mesozoic Oceans.** Summing up, we surmise that the low Mg/Ca ratio of Mesozoic seawater was due not only to increased high-T hydrothermal circulation in basalt and to enhanced dolomite deposition, but also to the quasi-absence of seawater/mantle peridotite reactions in the Mesozoic. Significant Mg input to seawater due to hydration of mantle rocks must have started after
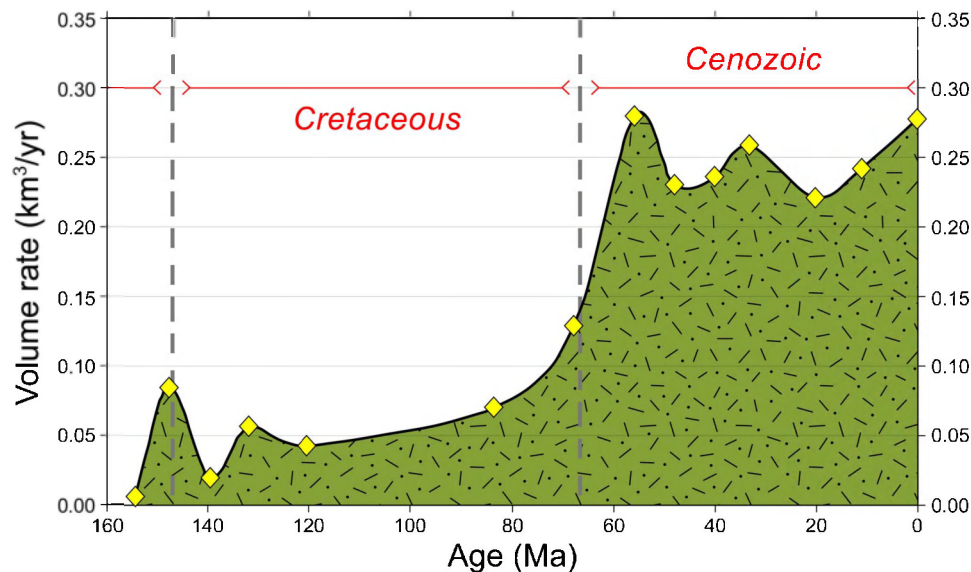
**Figure 5 | Temporal variations of volume of mantle rocks that may react with seawater at T < 150°C along mid-ocean ridges since 150 Ma.**

the break up of the supercontinent and the gradual development of slow-spreading ridges in new intercontinental oceans. Based on plate tectonic reconstructions, a strong decrease in oceanic basaltic crust production and a sharp increase in MORP-seawater reactions occurred from the Santonian (anomaly M25, 83.5 Ma) to the late Paleocene (c25, 55.9 Ma) (Fig. 5 and *Supplementary Information*). Reconstruction at 83.5 Ma suggests that mid-ocean ridges half spreading rate was then generally faster than 15 mm/yr (Fig. 2b), with scarce possibility of low-T MORP-seawater reactions and of Mg release to seawater (Fig. 3). Different stretches of slow spreading ridges, with significant MORP exposures, became active at different times: Mg release to seawater must have increased accordingly. The Mid Atlantic Ridge/megatransform system, a major potential source of Mg, developed 80–100 Ma. The Gakkel Ridge-Lena Trough segments, with broad exposure of ultramafics[56,67], developed about 53 Ma and 10 Ma, respectively[68]. The SWIR from ∼ 50° E to the Rodriguez triple junction, today a major MORP contributor, developed from ∼ 60 Ma to today[69]. The Andrew Bain megatransform in the SWIR, today a significant locus of ultramafic exposures, developed not earlier than about 50 Ma[70].

## Discussion

The cumulative increase of the quantity of MORP available to interact with seawater in the post-Mesozoic oceans (Figs. 1 and 5) parallels the increase of seawater Mg/Ca ratio documented by ref. 8. A >20% volume fraction of those MORPs potentially able to interact with seawater would help explain the Tertiary increase of Mg concentration in seawater (Fig. 1c) inferred from halite fluid inclusions[3–5].

Model results suggest that three important processes have affected temporal variations of Mg/Ca during the last 150 Ma: (1) hydrothermal circulation in basalts; (2) low-temperature MORP/seawater reactions; and (3) dolomite formation. Variations of oceanic crust production imply variations of Mg-removal and Ca-release by hydrothermal circulation in basalt. Given that the calculated oceanic crust production was higher during the Cretaceous than in the Cenozoic, we estimated a greater hydrothermal Mg-uptake and Ca-release in the Cretaceous than in the Cenozoic. We have shown that Mg-input to seawater due to Mg-release by MORP/seawater reactions was low (less than 4% of the river input) during the Cretaceous and high (up to 20% of the river input) during the Cenozoic. In addition, we have shown, from Mg isotope budget

constraints, that Mg-capture by dolomite precipitation was higher during the Cretaceous (up to 23% of the river input) than during the Cenozoic (down to 14% of the river input). We conclude that the absence of Mesozoic MORP-seawater reactions, followed by their increasing importance, contributed significantly to the increase of seawater Mg/Ca ratio from the Mesozoic to the modern oceans.

## Methods

**Mg model.** We assume a model where secular variations of seawater Mg-content are controlled by: (1) a constant influx from rivers; (2) variable Mg-release flux from peridotite-seawater reactions; (3) variable Mg-removal flux from high-temperature hydrothermal alteration of the basaltic crust as the result of seafloor spreading rate variations; and (4) a constant Mg residual-outflow including low-temperature off-axis hydrothermal interactions, deposition of dolomite, ion-exchange reactions with clays. Changes in the size of the oceanic Mg reservoir are thus calculated as:

$$\frac{d[Mg]}{dt} = F_{rw}^{Mg} + F_{hyP}^{Mg}(t) - F_{hyB}^{Mg}(t) - F_{res}^{Mg} \qquad (1)$$

where: $F_{rw}^{Mg}$ is the constant river influx, assumed of $5.6 \cdot 10^{12}$ mol/yr; $F_{hyP}^{Mg}(t)$ is the influx due to MORP-seawater reactions. We let the MORP-derived Mg flux vary through time following the estimated volume of mantle rocks that can interact yearly with seawater at T < 150°C (Fig. 5). The estimated recent flux is of $1.15 \cdot 10^{12}$ mol/yr, assuming that 100% of MORPs that can potentially react with seawater at T < 150°C do actually react and lose 5% wt of their MgO content (i.e., $F_{hyP}^{Mg}(0) = 0.05 \cdot \rho_m \cdot P_m(0)/ [MgO_{molar \; mass}]$, where $\rho_m = 3300$ kg/m³ is the density of mantle rocks and $P_m(0) = 2.7769 \cdot 10^8$ m³/yr is the current volume rate of MORP that interact with seawater at T < 150°C); $F_{res}^{Mg}$ is a constant unknown Mg-residual outflow; and $F_{hyB}^{Mg}(t) = H_{hT}(t) \, [Mg]_{sw}(t)$ is the Mg-removal flux at time $t$ by high-T hydrothermal circulation ($H_{hT}$) at ridge axis, that varies due to variations in the rate of seafloor production (*Supplementary Tab. S5*). $[Mg]_{sw}(t)$ is the concentration of Mg in seawater at time $t$. $H_{hT}(0)$ is the modern mid ocean ridge high-T hydrothermal flux, assumed at $5 \cdot 10^{13}$ kg/yr. Assumed values of 3 and $5.2 \cdot 10^{13}$ kg/yr (range of the estimated high-T hydrothermal flux) do not change our main results.

**Ca model.** Secular variations of seawater Ca-content have been modelled assuming: a constant river influx $F_{rw}^{Ca}$ of $1.4 \cdot 10^{13}$ mol/yr; a variable net influx $\tilde{F}_{hyB}^{Ca}(t)$ due to Ca capture/release during low and high temperature hydrothermal circulation in mid ocean ridge basalts; a variable outflux $F_{wMORP}^{Ca}(t)$ related to MORP alteration at seafloor; and an unknown constant residual Ca-outflow $F_{res}^{Ca}$ including: Ca-fixation due to carbonate accumulation (biogenic and inorganic), and anhydrite precipitation. Thus, changes through time of seawater Ca-content can be described by:

$$\frac{d[Ca]}{dt} = F_{rw}^{Ca} + F_{hyB}^{Ca}(t) - F_{wMORP}^{Ca}(t) - F_{res}^{Ca} \qquad (2)$$

We assume that secular variations of the net flux $F_{hyB}^{Ca}(t)$ due to Ca-release by hydrothermal circulation and Ca-capture by MORB alteration follow variations of oceanic crust production (*Supplementary Tab. S5*), with a modern MORB

hydrothermal-weathering net inflow $F_{hyB}^{Ca}(0)$ of $1.25 \cdot 10^{12}$ mol/yr. Assumed values of $0.8 \cdot 10^{12}$ and $1.5 \cdot 10^{12}$ mol/yr (range of the estimated hydrothermal flux) do not change our main results. In addition, we assume variations through time of Ca-removal by MORP weathering $F_{wMORP}^{Ca}(t)$ that scales linearly with variations in volume of mantle rocks that can interact yearly with seawater at $T < 150°C$ (Fig. 5 and *Supplementary Tab. S5*).

Numerical solutions of eqs. (1) and (2) were reached by finite difference approximation (Crank-Nicolson implicit scheme) using an integration time step of 1 Ma and initial (150 Ma) Mg- and Ca-seawater concentrations ([Mg] = 30.5 mmol/kg $H_2O$ and [Ca] = 24 mmol/kg $H_2O$), inferred from halite fluid inclusions[5]. The unknown residual fluxes $F_{res}^{Mg}$ and $F_{res}^{Ca}$ were solved iteratively to fit the modern Mg- and Ca-seawater concentrations ([Mg] = 53 mmol/kg $H_2O$ and [Ca] = 10.5 mmol/kg $H_2O$). Model details are presented in *Supplementary Information*.

1. Wilkinson, B. H. & Algeo, T. J. Sedimentary carbonate record of calcium-magnesium cycling. *Am. J. Sci.* **289**, 1158–1194 (1989).

2. Morse, J. W., Wang, Q. & Tsio, M. Y. Influence of temperature and Mg: Ca ratio on $CaCO_3$ precipitation from seawater. *Geology* **25**, 85–87 (1997).

3. Zimmerman, H. Tertiary seawater chemistry: implications from primary fluid inclusions in marine halite. *Am. J. Sci.* **300**, 723–767 (2000).

4. Lowenstein, T. K., Timofieff, M. N., Brennan, S. T., Hardie, L. A. & Demicco, R. M. Oscillations in Phanerozoic seawater chemistry: evidence from fluid inclusions. *Science* **294**, 1086–1088 (2001).

5. Horita, J., Zimmermann, H. & Holland, H. D. Chemical evolution of seawater during the Phanerozoic: implications from the record of marine evaporites. *Geochim. Cosmochim. Acta* **66**, 3733–3756 (2002).

6. Holland, H. D. Sea level, sediments and the composition of seawater. *Am. J. Sci.* **305**, 220–239 (2005).

7. Holland, H. D. & Zimmerman, H. The dolomite problem revisited. *Int. Geol. Rev.* **42**, 481–490 (2000).

8. Coggon, R. M., Teagle, A. H. D., Smith-Duque, C. E., Alt, J. C. & Cooper, M. J. Reconstructing past seawater Mg/Ca and Sr/Ca from mid-Ocean Ridge flank calcium carbonate veins. *Science* **327**, 1114–1117 (2010).

9. Broecker, W. & Yu, J. What do we know about the evolution of Mg to Ca ratios in seawater? *Paleoceanography* **26**, PA3203, doi:10.1029/2011PA002120 (2011).

10. Coggon, R. M., Teagle, A. H. D. & Jones, T. D. Comment on "What do we know about the evolution of Mg to Ca ratios in seawater?" by Wally Broecker and Jimin Yu. *Paleoceanography* **26**, PA3224, doi: 10.1029/2011PA002186 (2011).

11. Hardie, L. A. Secular variation in seawater chemistry: an explanation for the coupled secular variation in the mineralogies of marine limestones and potash evaporites over the past 600 m.y. *Geology* **24**, 279–283 (1996).

12. Demicco, R. V., Lowenstein, T. K., Hardie, L. A. & Spencer, R. J. Model of seawater composition for the Phanerozoic. *Geology* **33**, 877–880 (2005).

13. Paris, G., Gaillardet, J. & Louvat, P. Geological evolution of seawater boron isotopic composition recorded in evaporites. *Geology* **38**, 1035–1038 (2010).

14. Drever, J. I. The magnesium problem. In The Sea. Vol **5**, edited by Golberg, E. D. 337–357, Wiley Interscience (1974).

15. Edmond, J. M. et al. Ridge crest hydrothermal activity and the balances of the major and minor elements in the ocean: the Galapagos data. *Earth Planet. Sci. Lett.* **46**, 1–18 (1979).

16. Elderfield, H. & Schultz, A. Mid-ocean ridge hydrothermal fluxes and the chemical composition of the oceans. *Annu. Rev. Earth Planet. Sci.* **24**, 191–224 (1996).

17. Teagle, D. A. H., Bickle, M. J. & Alt, J. C. Recharge flux to ocean-ridge black smoker systems:Ageochemical estimate from ODPHole 504B. *Earth Planet. Sci. Lett.* **210**, 81–89 (2003).

18. Nielsen, S. G. et al. Hydrothermal fluid fluxes calculated from the isotopic mass balance of thallium in the ocean crust. *Earth Planet. Sci. Lett.* **251**, 120–133 (2006).

19. Vance, D., Teagle, D. A. H. & Foster, G. L. Variable Quaternary chemical weathering fluxes and imbalances in marine geochemical budgets. *Nature* **458**, 493–496 (2009).

20. Mottle, M. J. & Wheat, C. G. Hydrothermal circulation through Mid Ocean Ridge flanks: fluxes of heat and magnesium. *Geochim. Cosmochim. Acta* **58**, 2225–2237 (1994).

21. Elderfield, H., Wheat, G. C., Mottl, M. J., Monnin, C. & Spiro, B. Fluid and geochemical transport through ocean crust: A transect across the eastern flank of the Juan de Fuca Ridge. *Earth Planet. Sci. Lett.* **172**, 151–165 (1999).

22. Wheat, C. G. & Mottle, M. J. Composition of pore and spring waters from Baby Bare: Global implications of geochemical fluxes from a ridge flank hydrothermal system. *Geochim. Cosmochim. Acta* **64**, 629–642 (2000).

23. Schramm, B., Devey, C. W., Gillis, K. M. & Lackschewitz, K. Quantitative assessment of chemical and mineralogical changes due to progressive low-temperature alteration of East Pacific Rise basalts from 0 to 90 Ma. *Chemical Geology* **218**, 281–313 (2005).

24. Wolery, T. J. & Sleep, N. H. Hydrothermal circulation and geochemical flux at Mid Ocean Ridges. *J. Geol.* **84**, 249–275 (1976).

25. Hamley, J. J., Montoya, J. W., Christ, C. L. & Hostetler, P. B. Mineral equilibria in the MgO-$SiO_2$-$H_2O$ system: Talc-chrysotile-forsterite-brucite stability reactions. *Am. J. Sci.* **277**, 322–351 (1977).

26. MacDonald, A. H. & Fyfe, W. S. Rate of serpentinization in sea floor environments. *Tectonophysics* **116**, 123–135 (1985).

27. O'Hanley, D. S. Serpentinites: recorders of tectonic and petrological hystory. *Oxford Monograph on Geology and Geophysics* **34**, 290, Oxford University Press, New York (1996).

28. Frost, B. R. & Beard, J. S. On silica activity and serpentinization. *J. Petrol.* **48**, 1351–1368 (2007).

29. Klein, F. & Bach, W. Fe-Ni-Co-O-S phase relations in peridotite-seawater interactions. *J. Petrol.* **50**, 37–59 (2009).

30. Hostetler, P. B., Coleman, R. G., Mumpton, F. A. & Evans, B. W. Brucite in alpine serpentinites. *American Mineralogist* **51**, 75–98 (1966).

31. Bishoff, J. & Seyfried, W. E. Hydrothermal chemistry of sea water from 25°C to 350°C. *Am. J. Sci.* **278**, 838–860 (1978).

32. Seyfried, W. E. & Dibble, W. E. Seawater-peridotite interaction at 300°C and 500 bars: implications for the origin of oceanic serpentinites. *Geochim. Cosmochim. Acta* **44**, 309–321 (1980).

33. Janecky, D. R. & Seyfried, W. E. Hydrothermal serpentinization of peridotite within the oceanic crust: experimental investigations of mineralogy and major element chemistry. *Geochim. Cosmochim. Acta* **50**, 1357–1378 (1986).

34. Snow, J. E. & Dick, H. J. B. Pervasive magnesium loss by marine weathering of peridotite. *Geochim. Cosmochim. Acta* **59**, 4219–4235 (1995).

35. Marcaillou, C., Munoz, M., Vidal, O., Parra, T. & Harfouche, M. Mineralogical evidence for $H_2$ degassing during serpentinization at 300°C/300 bar. *Earth Planet. Sci. Lett.* **303**, 281–290 (2011).

36. Bach, W. & Klein, F. The petrology of seafloor rodingites: insights from geochemical reaction path modeling. *Lithos* **112**, 103–117 (2009).

37. Luce, R. W., Bartlett, R. W. & Parks, G. A. Dissolution kinetics of magnesium silicates. *Geochim. Cosmochim. Acta* **36**, 35–50 (1972).

38. Bonatti, E. et al. Mantle thermal pulses below the Mid-Atlantic Ridge and temporal variations in the formation of oceanic lithosphere. *Nature* **423**, 499–505 (2003).

39. Boschi, C. et al. Serpentinization of mantle peridotitesalong an uplifted lithospheric section, Mid Atlantic Ridge at 11° N. *Lithos* **178**, http://dx.doi.org/10.1016/j.lithos.2013.06.003 (2013).

40. Boschi, C., Dini, A., Früh-Green, G. & Kelley, D. S. Isotopic and element exchange during serpentinization and metasomatism at the Atlantis Massif (MAR 30°N): insights from B and Sr isotope data. *Geochim. Cosmochim. Acta* **72**, 1801–1823 (2008).

41. Niu, Y. Bulk-rock major and trace element compositions of abyssal peridotites: Implications for mantle melting, melt extraction and post-melting processes beneath mid-ocean ridges. *J. Petrol.* **45**, 2423–2458 (2004).

42. Boschi, C. Building Lost City: serpentinization, mass transfer, and fluid flow in an oceanic core complex. Ph.D. Thesis, ETH 16720, Zurich (2006).

43. Chen, Y. J. Oceanic crustal thickness versus spreading rate. *Geophys. Res. Lett.* **19**, 753–756 (1992).

44. Ligi, M., Cuffaro, M., Chierici, F. & Calafato, A. Three-dimensional passive mantle flow beneath mid-ocean ridges: an analytical approach. *Geophys. J. Int.* **175**, 783–805 (2008).

45. DeMets, C., Gordon, R. G. & Argus, D. F. Geologically current plate motions. *Geophys. J. Int.* **181**, 1–80 (2010).

46. Solomon, S. C., Huang, P. Y. & Meinke, L. The seismic moment budget of slowly spreading ridges. *Nature* **334**, 58–60 (1988).

47. Muller, R. D., Sdrolias, M., Gaina, C. & Roest, W. R. Age, spreading rates, and spreading asymmetry of the world's ocean crust. *Geochem. Geophys. Geosyst.* **9**, Q04006, doi:10.1029/2007GC001743 (2008).

48. Seton, M. et al. Global continental and ocean basin reconstructions since 200 Ma. *Earth Sci. Rev.* **113**, 212–270 (2012).

49. Bonatti, E. et al. Diffuse impact of the Mid Atlantic Ridge with the Romanche transform: an Ultracold Ridge/Transform Intersection. *J. Geophys. Res.* **101**, 8043–8054 (1996).

50. Bonatti, E. et al. Steady-state creation of crust-free lithosphere at cold spots in mid-ocean ridges. *Geology* **29**, 979–982 (2001).

51. Dick, H. J. B., Lin, J. & Schouten, H. An ultraslowspreading class of ocean ridge. *Nature* **426**, 405–412 (2003).

52. Escartín, J. et al. Central role of detchment faults in accretion of slow-spreading oceanic lithosphere. *Nature* **455**, 790–794 (2008).

53. Smith, D. K., Escartin, J., Schouten, H. & Cann, J. R. Fault rotation and core complex formation: significant processes in seafloor formation at slow-spreading midocean ridges (Mid-Atlantic Ridge, 13–15°N). *Geochem. Geophys. Geosys.* **9**, Q03003. doi:10.1029/2007GC001699 (2008).

54. Bonatti, E. et al. Flexural uplift of a Lithospheric Slab near the Vema Transform (Central Atlantic): Timing and Mechanisms". *Earth Planet. Sci. Lett.* **242**, 642–655 (2005).

55. Cannat, M. et al. Thin crust, ultramafic exposures, and rugged faulting patterns at the the Mid-Atlantic Ridge (22°–24°N). *Geology* **23**, 49–52 (1995).

56. Michael, P. J. et al. Magmatic and amagmatic seafloor generation at the ultraslow-spreading Gakkel ridge, Arctic Ocean. *Nature* **423**, 956-U1 (2003).

57. Cannat, M. et al. Modes of seafloor generation at a melt-poor ultraslow-spreading ridge. *Geology* **34**, 605–608 (2006).

58. Hekinian, R. et al. Petrology of the East Pacific Rise crust and upper mantle exposed in the Hess Deep (eastern equatorial Pacific). *J. Geophys. Res.* **98**, 8069–8094 (1993).

59. Hékinian, R., Bideau, D., Hébert, R. & Niu, Y. Magmatism in the Garrett transform fault (East Pacific Rise near 13°27′S). *J. Geophys. Res.* **100**, 163–10,185 (1995).

60. Whitmarsh, R. B., Manatschal, G. & Minshull, T. A. Evolution of magma-poor continental margins from rifting to seafloor spreading. *Nature* **413**, 150–154 (2001).

61. Gurnis, M. Large-scale mantle convection and the aggregation and dispersal and supercontinents. *Nature* **332**, 695–699 (1988).

62. Stampfli, G. M. & Borel, G. D. A plate tectonic model for the Paleozoic and Mesozoic constrained by dynamic plate boundaries and restored synthetic oceanic isochrons. *Earth Planet. Sci. Lett.* **196**, 17–33 (2002).

63. Vils, F., Tonarini, S., Kalt, A. & Seitz, H.-M. Boron, lithium and strontium isotopes as tracers of seawater–serpentinite interaction at Mid-Atlantic ridge, ODP Leg 209. *Planet. Sci. Lett.* **286**, 414–425 (2009).

64. Tipper, E. T. *et al.* The magnesium isotope budget of the modern ocean: constraints from riverine magnesium isotope ratios. *Earth Planet. Sci. Lett.* **250**, 241–253 (2006).

65. Teng, F.-Z. *et al.* Magnesium isotopic composition of the Earth and chondrites. *Geochim. Cosmochim. Acta* **74**, 4150–4166 (2010).

66. Veizer, J. *et al.* $^{87}Sr/^{86}Sr$, $\delta^{13}C$ and $\delta^{18}O$ evolution of Phanerozoic seawater. *Chem. Geol.* **161**, 59–88 (1999).

67. Snow, J. E. *et al.* Oblique nonvolcanic seafloor spreading in Lena Trough, Arctic Ocean. *Geochem. Geophys. Geosyst.* **12**, Q10009, doi:10.1029/2011GC003768 (2011).

68. Blythe, A. E. & Kleinspehn, K. L. Tectonically versus climatically driven Cenozoic exhumation of the Eurasian plate margin, Svalbard: fission track analysis. *Tectonics* **17**, 621–639 (1998).

69. Patriat, P. & Segoufin, J. Reconstruction of the Central Indian Ocean. *Tectonophysics* **155**, 211–234 (1988).

70. Sclater, J. G., Grindlay, N. R., Madsen, J. A. & Rommevaux-Jestin, C. Tectonic interpretation of the Andrew Bain transform fault: Southwest Indian Ocean. *Geochem. Geophys. Geosyst.* **6**, Q09K10, doi:10.1029/2005GC000951 (2005).

71. Rausch, S., Böhm, F., Bach, W., Klügel, A. & Eisenhauer, A. Calcium carbonate veins in ocean crust record a threefold increase of seawater Mg/Ca in the past 30 million years. *Earth Planet. Sci. Lett.* **362**, 215–224 (2013).

72. Steuber, T. & Rauch, M. Evolution of the Mg/Ca ratio of Cretaceous seawater: Implications from the composition of biological low Mg calcite. *Mar. Geol.* **217**, 199–213 (2005).

73. Timofeeff, M. N., Lowenstein, T. K., da Silva, M. A. M. & Harris, N. B. Secular variation in the major-ion chemistry of seawater: Evidence from fluid inclusions in Cretaceous halites. *Geochim. Cosmochim. Acta* **70**, 1977–1994 (2006).

## Acknowledgements

## Author contributions

E.B. and M.L. developed the ideas and the methods for this study and wrote jointly the paper. M.C. carried out the geophysical modelling. D.B. processed the geochemical data on the peridotites. All the authors discussed extensively the results and the interpretations.

## Additional information

**Supplementary information** accompanies this paper at http://www.nature.com/scientificreports

**Competing financial interests:** The authors declare no competing financial interests.

**How to cite this article:** Ligi, M., Bonatti, E., Cuffaro, M. & Brunelli, D. Post-Mesozoic Rapid Increase of Seawater Mg/Ca due to Enhanced Mantle-Seawater Interaction. *Sci. Rep.* **3**, 2752; DOI:10.1038/srep02752 (2013).